# Location of the Pupil-Iris Border in Slit-Lamp Images of the Cornea

Nicola Ritter
Centre for Ophthalmology and Visual Science
The University of Western Australia
Nedlands, W.A., Australia, 6907
nritter@cyllene.uwa.edu.au

James Cooper
School of Computer & Information Science
Edith Cowan University
Mt. Lawley, W.A., Australia, 6050
j.cooper@cowan.edu.au

Robyn Owens
Department of Computer Science
The University of Western Australia
Nedlands, W.A., Australia, 6907
robyn@cs.uwa.edu.au

Paul P. van Saarloos
Centre for Ophthalmology and Visual Science
The University of Western Australia
Nedlands, W.A., Australia,6907
paulvs@cyllene.uwa.edu.au

## Abstract

*We present results for an active contour that finds the pupil-iris border in slit lamp images of the eye. Preprocessing involves producing a variance image from the original image and then locating the annulus, of a given size, which has the lowest mean variance. The centre of this annulus falls inside the pupil, giving a starting position for a discrete circular active contour (DCAC). The DCAC is moved under the influence of two forces—external and internal. The external force is based on the grey-scales immediately inside and outside of the contour, at each vertex, in both the original and variance images and pushes the vertices inwards. The internal force acts to move the contour towards a perfect polygon, $\delta$ larger than the current polygon. Repeated trials with decreasing values of $\delta$ are performed until equilibrium is reached between the two forces and the pupil/iris border has been found.*

## 1. Introduction

Slit lamp images such as those shown in Fig. 1 are used to study conditions and diseases of the cornea, iris and lens of the eye. They can be used to judge the relative thickness of the cornea and the size of the anterior chamber, and they can assist in diagnosis of such problems as edemas, precipitates, tumours, foreign bodies and perforations [11]. Multiple images need to be registered to allow the creation of a three dimensional picture of a problem area. In addition, photographs taken over time need to be registered to allow clinicians to investigate changes.

This report presents a method for locating the pupil-iris border in slit lamp images—a first step in registration. A point interior to the pupil is located from a variance image and then a discrete circular active contour (DCAC) is created with this point as its centre. The DCAC is then moved under the influence of internal and external forces until it reaches equilibrium.

## 2. Registration

Registration of slit lamp images of the eye, such as those in Fig. 1, is complicated by the different movements that affect the images, the reflections on the cornea and iris and the nature of the eye itself.

There are several movements that affect a series of corneal images. Although subjects rest their head on a chin support and against a forehead support, this cannot prevent small movements of the head, which result in movement of the entire eye from image to image. The eye also moves relative to the surrounding skin and eyelashes. This movement (which is approximately that of a ball-and-socket joint) takes the form of apparent $x$ and $y$ translations of the pupil and iris as well as rotation of these around the centre of the pupil. A third movement within the image occurs when subjects move their eyelids—at its extreme this movement results in a blink that will form an image that must be removed from any sequence. Fourthly, changes in light intensity affect the size of the pupil, causing the internal dimension of the iris to change. Finally the slit lamp reflections themselves move as the eye is scanned.

Further problems are caused by specular reflections, both those that are being used to illuminate the eye for the purpose of photography, and those of incidental light sources. The slit-lamp reflections—of which there are gen-

(a) Image of an eye showing the three light stripes formed by reflections of the iris (brightest) and front and back of the cornea. Images such as these can help diagnose diseases of the cornea, iris and lens.

(b) In this image the slit-lamp reflection from the iris has been 'interrupted' by the pupil and lens. There is also reflected light from the front and rear of the cornea obscuring the pupil-iris border.

Figure 1: Images of an eye taken with a Zeiss 40SLP photo slit lamp bio-microscope on to colour slides. The slides were then digitized using a Polaroid Sprint Scan 35 into grey-scale images of size $512 \times 239$ pixels. Registration of these images is made difficult by specular reflections, the indeterminate nature of the pupil-iris border, changes in the size of the pupil between images, the eyelashes and the slit-lamp reflections themselves. The 'fuzziness' at the rear of each reflection—most noticeable on that of the iris—is caused by *scatter* due to imperfections in the cornea and is a major diagnostic tool for locating disease in the eye.

erally three: off the front of the cornea, the rear of the cornea and the iris (the brightest)—also cause problems as they 'wash-out' the image data of the iris where they cross it and cause apparent distortions to the pupil-iris border. A second source of distortion is caused by eyelashes that hang down over the eye—whilst it is possible to tape eyelashes out of the way, to do so is unpleasant and intrusive for the subject.

The required registration needs to be based on the pupil and iris, not that of the surroundings of the eye. Traditional techniques involving template matching have difficulties with the automated selection of an 'interesting' template. Whole image techniques such as phase-based methods and mutual information can become 'confused' by features such as the eyelids and eyelashes, which move relative to the pupil.

Eye-tracking techniques either require complicated physical hardware setups [3], or are based on the use of infra-red image differencing methods [5] which are not appropriate for slit-lamp images as all details of the pupil surroundings, including the slit lamp reflections, are lost.

Other researchers (such as Moore *et al*. [14]) use a "centre-of-mass" method to find the pupil. First the image is thresholded so that the pupil appears as a black disc in a mostly white background and then the centroid of the black pixels is calculated to find an estimate of the centre of the pupil. This method fails when applied to slit lamp images because the light from the slit lamp causes some reflection from the lens, resulting in the pupil appearing less black than normal.

Ivins *et al*. [7] develop a method that uses a deformable model of the iris to measure movements of the eye using cross-correlation of iris signatures found in 3 arcs around the centre of the pupil. Unfortunately the results presented in the paper of Ivins *et al*. are only for a single image of an eye warped to produce a second image—this type of test registration will generally give spurious levels of success. This is particularly true in the case of the iris which is made up of muscles that are used to contract and dilate the pupil.The patterns on the iris are caused by light catching these muscles and will deform when the muscles move. This deformation will be local to the iris rather than global as produced by warping an entire image.

A further disadvantage of the method proposed by Ivins *et al*. is that it requires manual selection of the centre of the pupil in the first image: the repeatability of this may vary and it prevents full automation of the process. Finally, with slit lamp images, the light stripe itself will overlap parts of the iris, making it difficult to align the semi-circles of iris signature.

We propose a new method in which the inside of the pupil is roughly located by searching for the least variable part of the image. A discrete circular active contour is then applied to a combination of the intensity and variance images to find the pupil-iris border.

## 3. Active Contours

Active contours (or 'snakes') are used to find features in images. They are models that are defined by a spline [8, 18], a b-spline [13, 4], connected line segments [10] or nodes connected by 'springs' [12]. In response to internal and external forces defined by the researcher, they can deform internally as well as move across the image. The actual minimization of the energies can be accomplished in several ways such as an iterative approach using the calcu-

lus of variations combined with the solving of Euler equations [8, 13], dynamic programming [2] or greedy algorithms [17, 9].

The vertices of a contour are pushed around under the influence of two opposing forces, one of these formed from constraints internal to the contour and the other from constraints external to the contour, that is from the image. Therefore each vertex is moved between time $t$ and time $t+1$ by

$$v_i(t+1) = v_i(t) + F_i(t) + G_i(t), \qquad (1)$$

where $F_i$ is the internal force, $G_i$ is the external force and $v_i$ is the position of vertex $i$.

The internal forces are dependent on the characteristics that the researcher wishes to balance for the active contour. These include balance between the contour acting as a membrane as opposed to a thin plate [8, 2, 18], the curvature of the contour versus its continuity [17, 9], and the use of prior information about the object shape [6]. The external forces are generally found using either edge information [13, 2, 4] or statistics/probabilities about regions within the image [16, 15, 1].

Since we are searching for a round object (the pupil-iris border) we use this prior information to describe our active contour with an internal force pushing it to form a globally expanding discrete circle, in other words a perfect polygon. For the external force we cannot use edge detection, (see Fig. 2(a)) as edge-detection 'picks up' shading within the pupil producing edges that incorrectly attract the contour. An alternative is the variance image shown in Fig. 2(b) which does not have this limitation whilst still clearly defining the boundary between the pupil and iris. This external force pushes the contour inwards towards the current centroid. We call this contour a discrete circular active contour (DCAC).

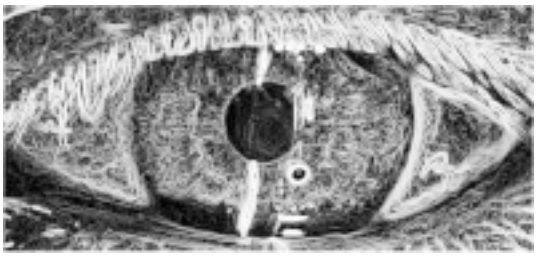

(a) A gradient or edge detection image (sobel) calculated from the image shown in Fig. 1(b) after histogram equalization has been performed. The edge detection has created contours within the pupil that 'distract' the DCAC from finding the pupil/iris border.

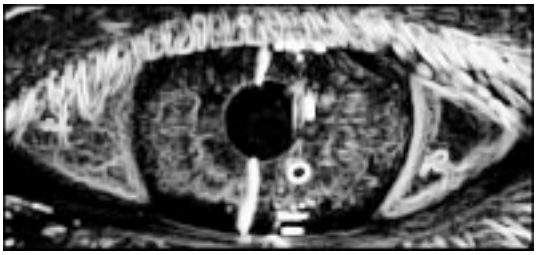

(b) A variance image calculated from the image of 1(b). Each pixel is the variance of a $5 \times 5$ window surrounding it. The image is then rescaled and histogram equalization is performed. The pupil appears as a smooth dark portion of the image.

Figure 2: These images are formed from processing the image shown in Fig. 1(b). The variance image gives a far more clearly defined border between the pupil and iris.

## 4. Preprocessing—Finding the Approximate Location of the Pupil

Active contours will only find nearby objects and closed contours need either to enclose or be contained by the object. For corneal images this necessitates finding a point interior to the pupil. As previously mentioned, averaging of the dark pixels will not necessarily find a point within the pupil because of the light reflected off the lens behind the pupil. However even where the pupil is lit there is still a 'smoothness' of texture differentiating it from the rest of the image. For this reason we chose to process the image with a variance filter—each pixel in the image is replaced with a grey-scale value calculated from the variance of a $5 \times 5$ square surrounding the pixel. The image is then rescaled to have 256 grey-scales and histogram equalization performed. An example of such an image can be seen in Fig. 2(b). A point interior to the pupil is then found by searching for the annulus that has the lowest mean variance of pixel grey-levels.

## 5. Discrete Circular Active Contour for Location of the Pupil-Iris Boundary

The DCAC is defined as a set of $n$ vertices, connected by line segments. The $n$ vertices are then positioned so as to form a perfect polygon within a circle with centre $\mathbf{p} = (r\ ,\ c)$ and radius $R$. The initial centre is that found with the algorithm of Section 4 and the initial radius is chosen to be less than any possible pupil size.

Each vertex $\mathbf{v}_i$ of the contour is then moved from time $t$

to $t+1$ using

$$\mathbf{v}_i(t+1) = \mathbf{v}(t) + \lambda \mathbf{F}_i(t) + (1-\lambda)\mathbf{G}_i(t) \quad \text{for all } i = 1 \ldots n, \tag{2}$$

where $\mathbf{F}_i$ is the force formed from the internal structure of the contour, $\mathbf{G}_i$ is that force produced by the information external to the contour—information from the grey-levels of the pixels in the images—and $n$ is the number of vertices. The constant $\lambda$ is used to balance the values and depends on the level of contrast in the images.

The internal force works to expand the contour from its current position into one with the same centroid but formed as a perfect polygon with a radius increased by $\delta$ from the current average radius. Therefore the internal force for each vertex is found with

$$\mathbf{F}_i = \tilde{\mathbf{v}}_i - \mathbf{v}_i, \tag{3}$$

where $\tilde{\mathbf{v}}_i$ is the position of this vertex in the perfect polygon. If $R$ is the average radius of the current contour and $\mathbf{p} = (r\ ,\ c)$ is the current centroid, then

$$\tilde{\mathbf{v}}_i = \begin{pmatrix} r - (R+\delta) * \sin\left(\frac{2\pi i}{n}\right), \\ c + (R+\delta) * \cos\left(\frac{2\pi i}{n}\right) \end{pmatrix}, \tag{4}$$

where $\delta$ is the increase in the radius at each iteration, the centroid $\mathbf{p}$ is defined by

$$\mathbf{p} = (r\ ,\ c) = \frac{1}{n}\sum_{i=1}^{n} \mathbf{v}_i, \tag{5}$$

the radius $R$ is defined by

$$R = \frac{1}{n}\sum_{i=1}^{n} \| \mathbf{v}_i - \mathbf{p} \|, \tag{6}$$

and $n$ is the number of vertices in the contour.

The external force pushes each vertex inwards towards the current centroid of the contour with a magnitude determined by both the original corneal image and the variance image. This ensures that both the darkness of the pupil and its even texture, as compared to the iris, are used to find the pupil-iris border.

However, problems with this external force are caused by the slit from the slit-lamp, specular reflections from other light sources and the high variance due to eyelashes; these all create forces with large magnitudes in places that do not correspond to the pupil-iris border. To prevent this from happening, the variance image is thresholded and inverted and the force at each vertex is multiplied by the resulting black (0) or white (1) pixel value for that vertex. This means that vertices affected by these problems have an external force of magnitude zero and react only to the influence of the internal force. Given that $I_1$ represents the original corneal image, $I_2$ the variance image and $I_3$ the thresholded and inverted variance image, then the external force is given by

$$\mathbf{G}_i(\mathbf{v}_i) = I_3(\mathbf{v}_i)\left(\psi \mathbf{G}_i(I_1, \mathbf{v}_i) + (1-\psi)\mathbf{G}_i(I_2, \mathbf{v}_i)\right), \tag{7}$$

where $\psi$ is a constant that balances the contribution of the original and variance images, and $I_j(\mathbf{v}_i)$ represents the nearest neighbour grey-scale value to the vertex $\mathbf{v}_i$ in image $I_j$. The external force $\mathbf{G}$ at a vertex $\mathbf{v}_i$ in an image $I_j$, is calculated from the grey-scale value of its current nearest neighbour and that of the nearest neighbour closest to the position it would take if moved one pixel inwards towards the current centroid of the contour. That is

$$\mathbf{G}_i(I_j, \mathbf{v}_i) = \mathbf{d}_i(I_j(\mathbf{v}_i) - I_j(\mathbf{v}_i + \mathbf{d}_i)), \tag{8}$$

where $\mathbf{d}_i$ is a unit vector given by

$$\mathbf{d}_i = \frac{\mathbf{p} - \mathbf{v}_i}{\| \mathbf{p} - \mathbf{v}_i \|}, \tag{9}$$

$\mathbf{p}$ being the centroid of the current contour, found with 5.

The movement of the contour continues for $M$ iterations or until it reaches one of the edges of the image. This process is repeated with decreasing values of $\delta$ until equilibrium occurs. This equilibrium is considered to have been reached if the average centre row, centre column and radius of the last $N$ iterations are less than $\varepsilon$ different from that of the previous $N$ iterations.

**Algorithm**

```
DO
    WorkingContour = StartingContour
    WHILE count < M
            AND WorkingContour is within the image
        Move WorkingContour
        Increment count by 1
    ENDWHILE
    Test for equilibrium
    Decrement δ by δ_c
UNTIL equilibrium is reached OR δ ⩽ 0
```

## 6. Results

The variables and constants that are required for our method are summarized in table 1, along with the values used.

Figure 4 shows graphs of the values of the centre row, centre column and radius of the contour over the $M$ iterations as a search is made for the pupil-iris border of Fig. 1(b). The graphs show decreasing values of $\delta$ and the reaching of equilibrium.

| | | |
|---|---|---|
| | The size of the square for producing the variance image | 5 |
| | The internal radius of the annulus | 17 |
| | The external radius of the annulus | 20 |
| | The threshold for the variance image | 150 |
| | The radius of the starting contour | 10 |
| $n$ | The number of vertices in the contour | 24 |
| $\delta$ | The initial value for the increment of the radius | 2.0 |
| $\delta_c$ | The amount by which $\delta$ is reduced if equilibrium was not reached, | 0.1 |
| $\lambda$ | The constant balancing the internal and external forces | 0.5 |
| $\psi$ | The constant balancing the contribution of the original and variance images to the magnitude of the external force | 0.9 |
| $M$ | The number of iterations | 1500 |
| $N$ | The number of iterations used to calculate the averages for testing for equilibrium | 250 |
| $\varepsilon$ | The maximum allowed difference between these averages | 1.0 |

Table 1: The variables required for implementation of our algorithm for finding the border between the pupil and the iris in slit-lamp images of the eye.

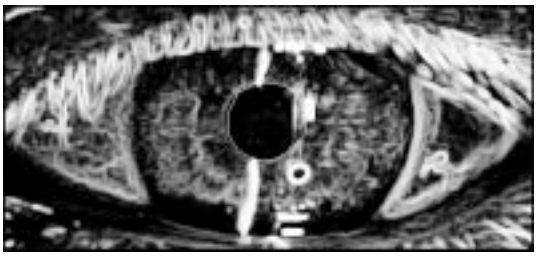

(a) The final contour for Fig. 1(b) after the process reached equilibrium, which occurred when $\delta = 0.8$, as can be seen in Fig. 4(c).

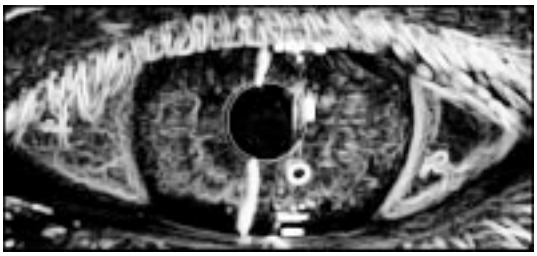

(b) The final circle found from averaging the contour shown in (a). This shows the accuracy of the algorithm.

Figure 3: The results of processing the image shown in Fig. 1(b).

Nine images of the same cornea were processed to find the pupil-iris border. Figure 3(a) shows the final contour for the image shown in Fig. 1(b) when $\delta = 0.8$—the value at which equilibrium is reached, as can be seen in Fig. 4. The success of the algorithm can be seen from the closeness of fit of the average circle calculated from this contour, and the actual pupil as shown in Fig. 3(b).

## 7. Conclusion

We describe a method of locating the pupil-iris border in slit-lamp images of the cornea. A Discrete Circular Active Contour is created, which moves under the influence of external and internal forces. The external force has a magnitude of either zero, where there is specular reflection, or is proportional to the difference between the grey-scales immediately inside and outside the contour at each vertex, in both the original and variance images. The internal force acts to move the contour to form a perfect polygon of radius $\delta$ more than the current average radius. The size of $\delta$ controls the magnitude of this force. If $\delta$ is too large the internal forces will 'overwhelm' the external forces and the border will not be found. If $\delta$ is too small the contour will never grow large enough. The 'perfect' value for $\delta$ varies from image to image, therefore a large value is chosen and reduced until there forms a stable equilibrium between the two forces.

The method is fully automated and deals with specular reflections, problems from eyelashes obscuring part of the pupil and the reflection from the slit-lamp itself.

Further work should enable the refinement of the result and the calculation of the rotation of the eye.

**Acknowledgments**
We would like to thank Chris Barry for allowing the use of the Zeiss 40SLP photo slit-lamp bio-microscope and for taking the images for us.
This work was supported by a Scholarship from The Lions Eye Institute of Perth, Western Australia.

## References

[1] J. 1vins and J. Porrill. Active region models for segmenting textures and colours. *Image and Vision Computing*, 13(5):431–438, June 1995.

[2] A. A. Amini, T. E. Weymouth, and R. C. Jain. Using dynamic programming for solving variational problems in vision. *IEEE Transactions on Pattern Analysis and Machine Intelligence*, 12(9):855–867, Sept. 1990.

[3] A. Davidhazy, T. Etoh, C. B. Johnson, D. R. Snyder, and J. S. Walton. Ultrahigh- and high-speed photography and image-based motion measurement. In *Proceedings of SPIE*, volume 3173, pages 249–261. SPIE, July 1997.

[4] P. Delanges, J. Benois, and D. Barba. Active contours approach to object tracking in image sequences with complex background. *Pattern Recognition Letters*, 16(2):171–178, Feb. 1995.

[5] Y. Ebisawa and M. Amano. Examination of eye-gaze detection technique using two light sources and the image difference method. In *SICE '94*, pages 985–990, July 1994.

[6] S. R. Gunn and M. S. Nixon. A robust snake implementation; a dual active contour. *IEEE Transactions on Pattern Analysis and Machine Intelligence*, 19(1):63–68, Jan. 1997.

[7] J. P. Ivins, J. Porrill, and J. P. Frisby. A deformable model of the human iris driven by non-linear least-squares minimisation. In *Sixth International Conference on Image Processing and its Applications IPA'97*, volume 1, pages 234–238, Dublin, 1997.

[8] M. Kass, A. Witkin, and D. Terzopoulos. Snakes: Active contour models. *International Journal of Computer Vision*, 4:321–331, 1988.

[9] K. M. Lam and H. Yan. Fast greedy algorithm for active contours. *Electronics Letters*, 30(1):21–23, Jan. 1994.

[10] S. Lobregt and M. A. Viergever. A discrete dynamic contour model. *IEEE Transactions on Medical Imaging*, 14(1):12–24, Mar. 1995.

[11] C. L. Martonyi, C. F. Bahn, and R. F. Meyer. *Clinical Slit Lamp Biomicroscopy and Photo Slit Lamp Biomicrography*. Time One Ink, Ltd, second edition, 1985.

[12] T. McInerney and D. Terzopoulos. Topologically adaptable snakes. In *Proceedings of the Fifth International Conference on Computer Vision (ICCV'95)*, pages 840–845, Cambridge, MA, USA, June 1995.

[13] S. Menet, P. Saint-Marc, and G. Medioni. Active contour models: Overview, implementation and applications. In *IEEE Conference on Systems, Man and Cybernetics*, pages 194–199. IEEE, 1990.

[14] S. T. Moore, T. Haslwanter, I. S. Curthoys, and S. T. Smith. A geometric basis for measurement of three-dimensional eye position using image processing. *Vision Research*, 36(3):445–459, 1996.

[15] R. Ronfard. Region-based strategies for active contour models. *International Journal of Computer Vision*, 13(2):229–251, Oct. 1994.

[16] G. Storvik. A bayesian approach to dynamic contours through stochastic sampling and simulated annealing. *IEEE Transactions on Pattern Analysis and Machine Intelligence*, 16(10):976–986, Oct. 1994.

[17] D. J. Williams and M. Shah. A fast algorithm for active contours and curvature estimation. *CVGIP: Image Understanding*, 55(1):14–26, Jan. 1992.

[18] G. Xu, E. Segawa, and S. Tsuji. Robust active contours with insensitive parameters. *Pattern Recognition*, 27(7):879–884, July 1994.

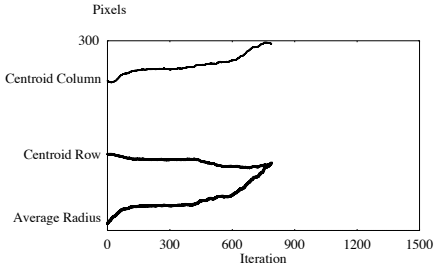


(a) A graph showing the changing values of the centre and radius of the contour as the iterations progress, when $\delta = 1.0$. The algorithm halts when the contour reaches the edge of the image.

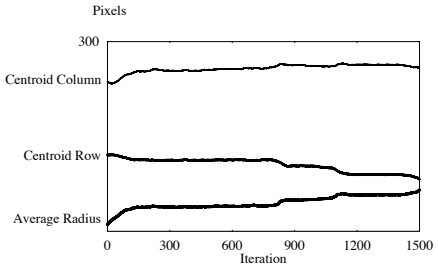


(b) When $\delta = 0.9$, the contour does not reach the edge of the image within the 1500 iterations, however it is clear that equilibrium has not been reached.

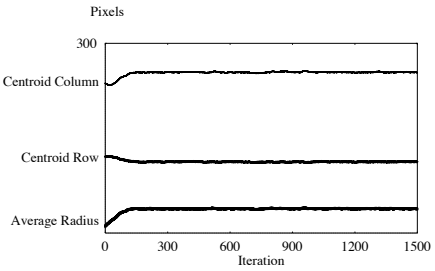


(c) $\delta$ is now 0.8 and the equilibrium of the contour is obvious from the graph. The accuracy of the circle found for the pupil-iris border can be seen in Fig. 3(b).

Figure 4: These graphs show the values of the centre of the contour (row and column) and its radius for each inner iteration of the algorithm. The three graphs show the changes that occur as $\delta$ is decreased the outer iteration of the algorithm. As $\delta$ decreases there is an increase in the number of inner iterations completed before the contour reaches the edge of the image, with equilibrium reached when $\delta = 0.8$.